A two-step method for rate-dependent nano-indentation of hydrogels

Polymer 137 (2018) 276–282

Contents lists available at ScienceDirect

Polymer

journal homepage: www.elsevier.com/locate/polymer

A two-step method for rate-dependent nano-indentation of hydrogels

Rok Simič, Christian H. Mathis [1], Nicholas D. Spencer*

Laboratory for Surface Science and Technology, Department of Materials, ETH, Zürich, Switzerland

ARTICLE INFO

Article history:
Received 17 November 2017
Received in revised form
31 December 2017
Accepted 5 January 2018
Available online 8 January 2018

Keywords:
Indentation
Contact mechanics
Soft matter
Hydrogels

ABSTRACT

Soft, biphasic materials such as hydrogels are commonly used to mimic lubrication and confinement mechanics of biological tissue such as articular cartilage or the cornea. In-depth understanding of such mechanics is crucial for designing synthetic replacements for cartilage, contact-lens materials or soft coatings for medical devices. Using colloidal-probe atomic force microscopy (AFM), surfaces can be investigated at the nanoscale and information on the contact modulus, poro-viscoelastic properties and the permeability can be extracted. Yet, probing the surface of a soft material in a liquid environment is challenging, since the point of contact between a probe and sample surface during finite-rate indentation can be obscured by viscous squeeze-out effects of temporarily confined liquid. To address this issue, we have developed a 2-step indentation method that enables accurate alignment of finite-rate indentation curves with respect to the contact point of quasi-static indentation of soft matter in liquid. In this work, the issue and the method are illustrated by measurements on a commonly used poly(acrylamide) (PAAm) hydrogel. We have shown that liquid squeeze-out may cause non-negligible force offsets that can result in false contact-point determination during finite-rate indentation. The presented method allows accurate alignment of the indentation curves, enables one to accurately study the rate-dependent contact moduli and related stiffening effects, and thus greatly facilitates mechanical characterization of both biological as well as synthetic soft materials.

1. Introduction

Biological tissues such as articular cartilage have been of interest to materials scientists and engineers for decades, due to their unique load-bearing and lubrication properties. The low friction and wear of articular layers has been attributed to the combined effect of different lubrication modes, including fluid-film lubrication by synovial fluid [1], boundary lubrication by a variety of molecules in synovial fluid [2], and lubrication by pressurisation of the interstitial fluid [3].

Several studies have demonstrated that interstitial fluid pressurisation leads to fluid load support, which strongly influences the frictional and mechanical response of cartilage [3–7]. Using rate-dependent indentation experiments allows one to study interstitial fluid pressurisation [8]. It was shown that bovine articular cartilage, with an equilibrium contact modulus of about 1 MPa, can effectively stiffen by a factor of six when fluid load support is involved. In fact, the fluid pressure can support up to 85% of the contact load when the cartilage is indented at a rate of several μm/s. This rate-dependent stiffening due to fluid pressurisation also explains the ability of cartilage to support contact stresses of up to 5 MPa occurring during normal joint usage [9]. In a related experiment, a direct correlation has been found between increasing fraction of total load supported by the fluid and decreasing friction coefficient [5].

The critical role of fluid load support has been demonstrated by degrading cartilage with proteolytic enzymes—known to cause degenerative changes that are comparable to the effects of osteoarthritis. This enzymatically treated cartilage showed increased friction and decreased effective contact modulus during rate-dependent indentation experiments [4]. Similarly, depleting cartilage of proteoglycans showed reduced contact moduli and fluid load support properties, when compared to a native, untreated cartilage in a nanoindentation study [10].

Improved understanding of the lubrication mechanics of biological tissue has inspired numerous studies focussing on comparable phenomena in synthetic materials, such as polymer brushes or hydrogels [11]. Studying synthetic materials is not only important for broadening our understanding of bio-lubrication, but is also

* Corresponding author.
E-mail address: nspencer@ethz.ch (N.D. Spencer).
[1] Present Addresses. SuSoS AG, Lagerstrasse 14, CH-8600 Dübendorf, Switzerland.

https://doi.org/10.1016/j.polymer.2018.01.017
0032-3861/

crucial for designing synthetic replacements for cartilage, contact-lens materials or even coatings for medical instruments [12]. It was observed, for example, that both sliding and indentation at higher rates induce fluid confinement within micrometer-thick, surface-grafted poly(dodecyl methacrylate) brushes, provided that the viscosity of the surrounding liquid is sufficiently high [13]. The fluid confinement enhanced the effective contact modulus, presumably shielding the polymer from the effects of load, similarly to the situation with cartilage. This kind of behavior has been observed in several oil-compatible polymer brushes [14–16], but the ability to confine liquid is not only limited to viscous liquid environments. The phenomenon was also observed in the case of aqueous solvents, where chemical or physical interactions between the brush and the fluid enable fluid-load support and prevent direct contact between the brush-coated surfaces [17–19].

Colloidal-probe atomic force microscopy (CP-AFM) nano-indentation has become a widespread technique for studying the surface mechanical properties of soft matter [20–23]. For example, CP-AFM enables the probing of surfaces on the nanoscale and the extraction of information on poro-viscoelastic, permeability and frictional properties. However, probing surfaces of soft matter in a liquid environment is a challenging task, since the contact between a probe and sample surface can be obscured by viscous squeeze-out effects of temporarily confined liquid during finite-rate indentation [24–26]. The phenomenon of liquid squeeze-out and its effect on normal force during indentation is shown schematically in Fig. 1. The liquid confinement in the area between the probe and the hydrogel may be further amplified due to steric effects between individual polymer chains protruding into the solvent at the diffuse interface between the hydrogel and the liquid.

The drainage of liquid confined between a probe and surface-grafted PEG brushes was analysed by Charrault et al. [27]. The force-distance curves could in this case be aligned according to the hard compliance region at the complete compression of the brush, allowing the drainage forces to be identified and analysed by applying the slip models of Vinogradova [25]. The authors explained the obtained apparent slip values partially by deformation of the soft layer, partially by flow through the brush layer, and partially by flow below the nominal surface, permeating through the inherent roughness of the substrate.

In the case of macroscopic hydrogel layers, however, a hard substrate cannot be reached to serve as a reference for the force-indentation curve alignment, necessitating an alternative approach. To this end, we have developed a 2-step indentation method to accurately align any finite-rate indentation curves with respect to the quasi-static indentation, where the point of contact between a probe and soft material in liquid can be determined more unambiguously. The method presented in this work not only enables the accurate analysis of rate-dependent material properties beyond the point of contact, such as rate- and depth-dependent stiffening effects, but also allows one to study drainage forces and related phenomena such as boundary slip, permeation of the fluid or compliance of the surface. In this work, we present the method applied to common poly-(acrylamide) (PAAm) hydrogels. However, it can be used on a variety of soft materials in viscous liquids in order to accurately characterize rate-dependent poro-viscoelastic material properties. Moreover, the method becomes especially important in viscous fluids and for large probe radii, since the squeeze-out forces due to confinement scale linearly with viscosity and indentation rate, and with the square of the probe radius [25].

2. Experimental

2.1. PAAm hydrogel synthesis

The acrylamide (AAm, Sigma-Aldrich, St. Louis MO, USA, ≥ 99%) and cross-linker N,N′-methylenebisacrylamide (bis-AAm, Sigma-Aldrich, ≥ 99.5%)) were dissolved in Milli-Q water at concentrations of 7.5 wt% and 0.3 wt%, respectively. The free-radical polymerization was initiated by ammonium persulfate (APS, Merck Group, Darmstadt, Germany, GR for analysis) and catalysed by N,N,N′,N′-tetramethylethane-1,2 diamine (Sigma-Aldrich, ≥ 99%), at a concentration of 0.01 wt% each. The reacting solution was poured into a piranha-cleaned glass Petri dish to a height of 2 mm and left to completely polymerize. After polymerization, the gel was removed from the Petri dish and immersed in a large beaker full of HEPES buffer solution for 48 h, to remove unreacted reagents and allow swelling of the gel. The surface of the gel that had been in contact with the glass Petri dish was used for the indentation analyses.

2.2. The indentation method

Nanoindentation experiments were performed using an AFM (MFP3D™, Asylum Research, Santa Barbara, USA). The thermal-noise method was used to determine the normal spring constant ($k = 1.31$ N/m) of the Au-coated tipless cantilever (NSC-36, Mikromash, Estonia) [28]. A silica microsphere (GP0083, Whitehouse Scientific, Waverton, UK) with a radius of 43 μm was glued with UV-curable glue (Norland optical adhesive 63, Norland Products, Inc., Cranbury, NJ, USA) to the end of the tipless cantilever by means of a home-built micromanipulator. The spring constant was then corrected for the colloid position on the cantilever as $k' = k\ (L'/L)^3 = 1.85$ N/m, where L is the cantilever length and L' is the distance from the base of the cantilever to the colloid position [29]. All measurements were performed at room temperature of

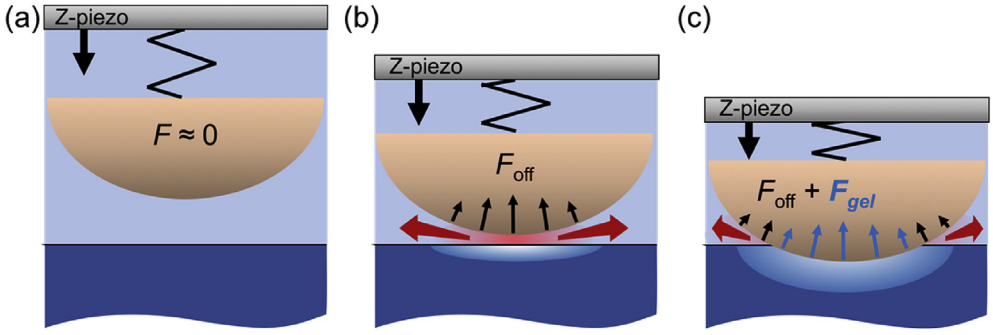

Fig. 1. Schematic of the liquid squeeze-out phenomenon during finite-rate indentation. (a) The probe experiences no forces related to liquid confinement, however, viscous drag may be present. (b) In the proximity of the surface, the probe experiences a force due to liquid squeeze-out. (c) Once in contact, a combination of forces due to squeeze-out effects and deformation of the hydrogel are acting on the probe.

22 °C ± 1 °C using a liquid cell with samples completely immersed in HEPES I buffer solution in order to control the electrostatic forces and minimize any capillary forces between the probe and the investigated surfaces. Prior to the measurements, the optical lever sensitivity was calibrated by pressing the probe against a hard surface of a silicon wafer in the same buffer solution to obtain the relation between the cantilever deflection and the photodiode signal. Using the buffer solution resulted in only negligible adhesion forces between the relatively large colloid and the silicon surface.

An acquisition rate of 2000 Hz was used, resulting in data points measured in time steps of $\Delta t = 0.5$ ms. Force maps of 5×5 force curves were obtained over an area of $20 \times 20\ \mu m^2$. Representative indentation curves are shown in the force plots, while the graphs in Fig. 5 depict averages of the force maps collected and subsequently analysed.

The method presented in this paper, however, does not depend on the device used, and can be applied to any kind of indentation that can be performed in liquid. It is based purely on the response of viscoelastic materials and phenomena occurring during a squeeze-out of confined fluid during a finite-rate approach of an indenter (of any shape) towards the tested material surface.

2.2.1. The two steps

Each indentation consisted of two steps. The first step comprised indentation at a finite rate up to a force set-point, Fig. 2a. The effective approach rates were set to be approximately 0.4, 2.0, 7.0, 40 and 70 μm/s, in order to cover a broad range of approach velocities. The actual approach rates of the piezo $z(t)$, were then precisely measured using a Z-piezo displacement sensor and used as such in further calculations. A set-point for the peak indentation force was set to $F_{max} = 210 \pm 5$ nN, which corresponds to 0.8−1.0 μm of indentation depth for the hydrogel used in this work. After reaching the set-point, the Z-piezo displacement was kept constant for 2.0 s to allow for force relaxation or equilibration. The selected equilibration time was sufficient for complete material relaxation. Rate-dependent visco- or poro-elastic contributions to the force initially sensed by the probe decayed by the end of the dwell period, at which point only the elastic contribution of the compressed hydrogel was measured. This not only allows for the analysis of the characteristic relaxation times, but also enables the correct execution of the second, slow step, which is used for depth alignment of the indentation curves.

Following the relaxation, the second step consisted of an additional piezo extension to a larger indentation depth at a slow rate of indentation, in order to exclusively probe the elastic response of the material. Fig. 2a depicts a schematic of a time-resolved force evolution, showing both the first and the second step of indentation. In the case of the PAAm hydrogel tested, a rate of 0.4 μm/s was sufficiently slow to result in no observable hysteresis between the extension and retraction parts of the curve, thus revealing the absence of any viscous response. However, the rate of the subsequent second step was set to an even lower value of 0.2 μm/s. The indentation depth of the second step needs to be sufficiently large to allow substantial overlap of all second steps of force-indentation curves obtained at either different rates and/or set-points during the first step.

The final indentation depth of the colloid after completion of the second step matches the depth reached at the end of the relaxation. Now the retraction rate was matched with the initial rate of indentation of the first step, allowing rate-dependent adhesion properties to be studied.

Fig. 2b shows how the force-distance curve obtained from the 2-step indentation shows firstly a classical force indentation profile followed by a dwelling period and the additional second step. This second, slow indentation allows for the precise depth alignment of the force-indentation curves obtained at different indentation rates applied during the first step. Through this, the point of contact between the probe and the surface can be precisely determined, despite the complicating hydrodynamic force offsets arising from possible drainage of the fluid between the probe and the sample surface [25,27,30].

2.2.2. Alignment of the curves

Individual indentation curves always require a baseline alignment, and in this methodology an additional alignment is

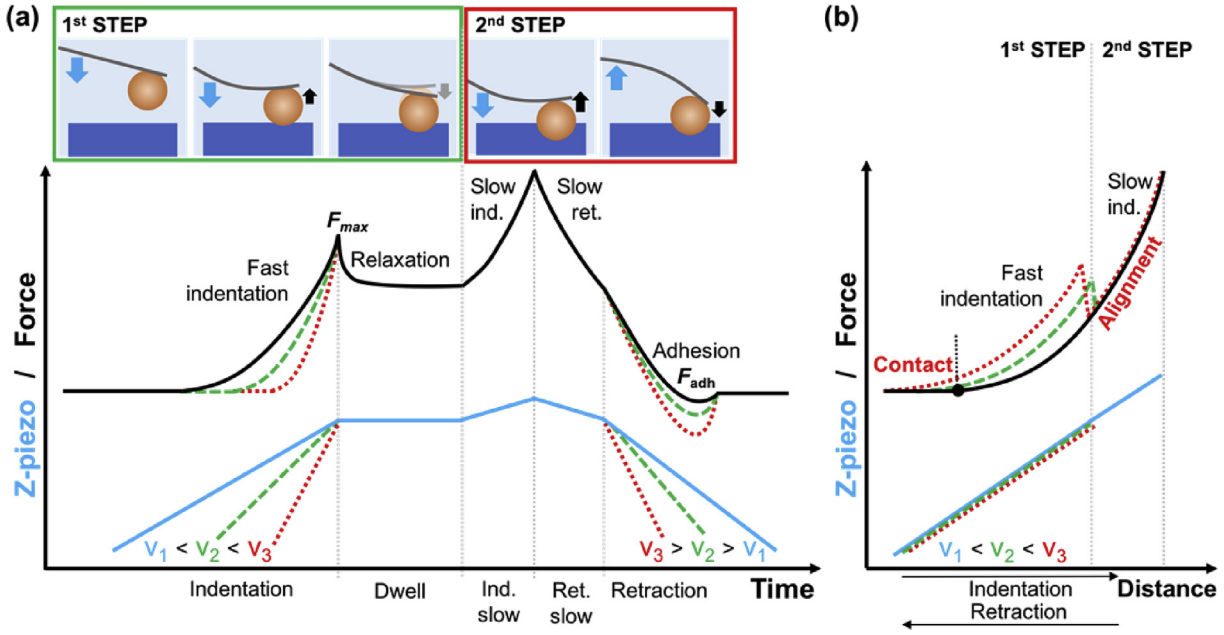

Fig. 2. Schematic of the rate-dependent, 2-step indentation method. Z-piezo displacement and force response as a function of (a) time and (b) indentation distance. Differences in force response after reaching F_{max} for the three rates are omitted in the time representation for reasons of clarity.

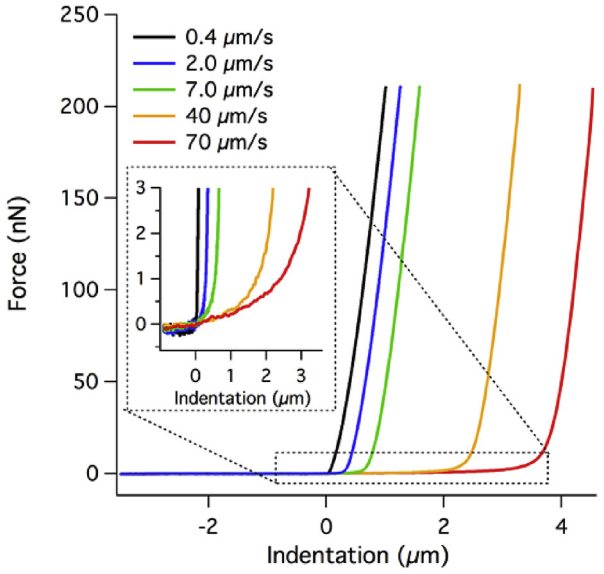

Fig. 3. Force curves at different rates, falsely aligned according to the distance point where force starts to deviate from zero by $2\sigma \sim 0.15\ nN$. The inset shows a magnified part of the graph around the alignment point. A misinterpretation of the contact point as a consequence of liquid confinement effects ahead of contact results in apparent increasing depth of indentation with increasing rate of approach.

performed with respect to the indentation depth, in order to accurately identify the point of contact between probe and sample surface. The alignment of the curves obtained at different rates was first performed in the direction of the force axis by subtracting the baseline from the force curve. In our case, the measured force due to the viscous drag acting on the colloid far from the surface should be negligible. To confirm that, the viscous drag acting on the colloidal probe while moving through the liquid was calculated. Taking into account the highest rate used, $v = 70\ \mu m/s$, the radius of the colloid, $R = 43\ \mu m$, the density of the aqueous buffer, $\rho = 10^6\ g/m^3$, and the kinematic viscosity of the buffer at 22 °C, $\eta = 0.9 \cdot 10^{-3}\ Pa \cdot s$, the Reynolds number yields a value of $Re = \frac{2Rv\rho}{\eta} = 0.007$, which is sufficiently low to assume laminar flow of the fluid around the colloid for all rates used in this work [31]. Consequently, the force acting on the colloid due to the viscous drag of the laminar flow is given by Stokes' law: $F_d = 6\pi\eta vR$ [32]. For the highest rate used, the calculated drag force was $F_d = 0.05\ nN$. Since the root-mean-square (RMS) of the noise in the force signal measured 0.07–0.08 nN in our experiments, the drag was assumed to be negligible in this case. The drag acting on the cantilever was indeed expected to be larger than the drag of the colloid due to the larger projected area of the cantilever compared to the colloid. However, the force read-out during the approach and retraction far from the surface did not show any significant difference [33,34]. Due to the absence of substantial drag, a linear function was fitted to the approach part far from the surface to account for any potential instrumental effects (e.g. virtual deflection). The fitted linear function was then extrapolated and subtracted from the entire force curve. This was carried out for all rates used in this work. In the case of higher rates or higher viscosities, a non-negligible difference in measured force during extension and retraction may arise. In this case, viscous drag needs to be evaluated and subtracted from the force curves accordingly [33,34].

After the force (y-axis) alignment, an alignment in the direction of the distance axis was performed. A definite point of contact between the probe and the surface of the sample was determined by evaluating the slowest indentation curve (*slow-rate*), assuming negligible effects due to fluid drainage close to the sample surface at this rate. Due to the absence of noticeable adhesive or repulsive electrostatic forces upon the approach, the point of contact was defined at the piezo position where force values started to diverge from zero (mean value far away from the surface) by more than two standard deviations of the force noise ($2\sigma \sim 0.15\ nN$). In general, other methods for contact-point determination during *quasi-static* indentation could be applied depending on the type of contact (e.g. adhesive or repulsive) [35,36].

If the curves for all higher rates (*fast-rate*), previously aligned in the force direction, were simply aligned in the distance direction in the same way as the *slow-rate* curves (e.g. force deviation from zero), a false interpretation of indentation depth would be made due to the liquid confinement and squeeze-out effects ahead of the contact, Fig. 3.

To avoid the misinterpretation of the contact point by solely determining the start of force deviation (Fig. 3), all *fast-rate* curves, previously aligned in the force direction, can be accurately aligned in the distance direction such that the second, slow-indentation, step of the force-indentation curve overlaps with the second step of the slow-rate curve, Fig. 4. Due to the absence of any adhesion forces upon approach in the present study, the overlapping was performed by fitting the second step of the slow-rate force-indentation curve using the Hertzian model [37]:

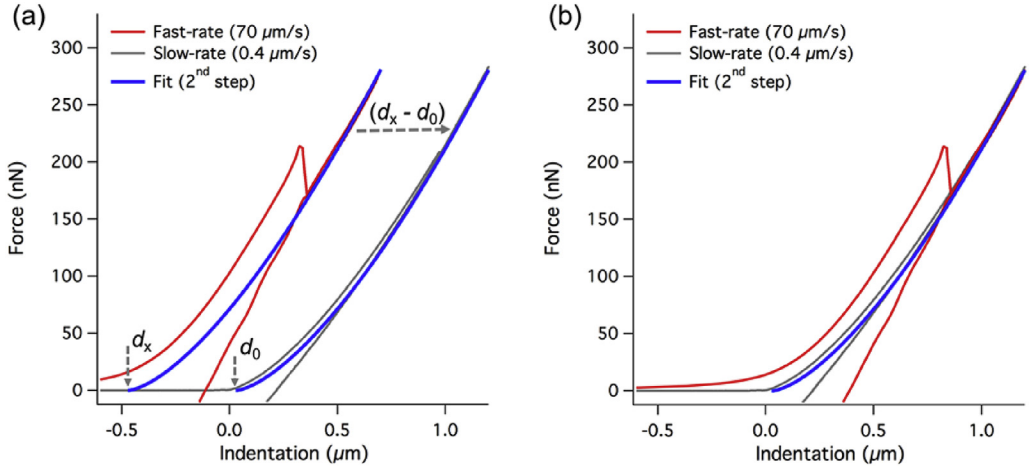

Fig. 4. Alignment procedure of the fast-rate curves to the slow-rate curve. (a) The second step of both curves is fitted with the same function, but with different offsets d_x and d_0 in the horizontal direction for the fast and slow rate, respectively. The fast-rate curve is then shifted for d_x - d_0 to align the curves. (b) Aligned curves.

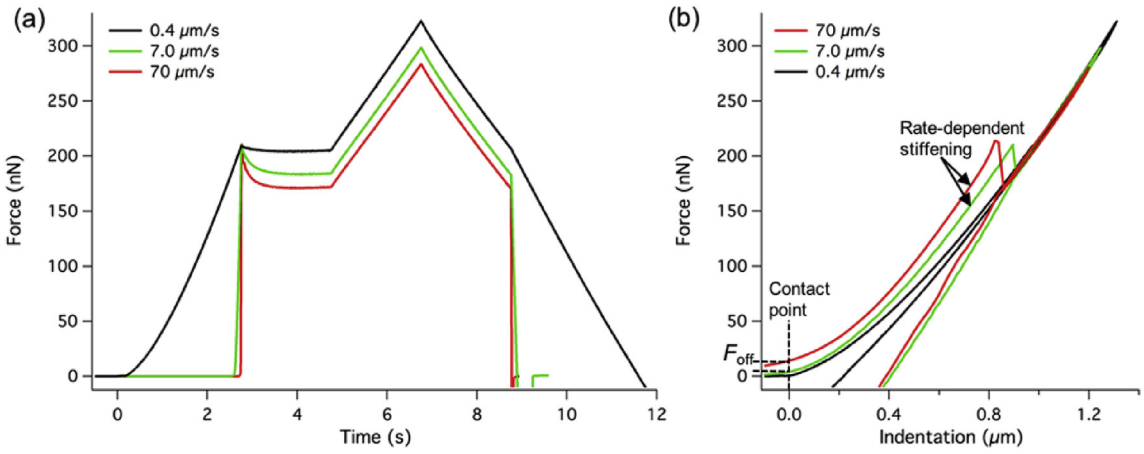

Fig. 5. Representative force curves upon indenting a PAAm hydrogel as a function of (a) time and (b) indentation distance.

$$F = \frac{4}{3}\frac{E\sqrt{R}}{1-\nu^2}(d-d_0)^{1.5}. \quad (1)$$

Here, F is the measured force, E is elastic modulus, ν is Poisson's ratio, and d is the indentation depth. To account for the deviations in force response from the classical Hertzian model (e.g. softer surface layer), an indentation offset d_0 was introduced, Fig. 3a. The Poisson's ratio was set to 0.5—a value used for comparable soft materials [27,35]. The obtained modulus E was then used to fit the second step of the faster-rate curves with the same model, but shifted by d_x:

$$F = \frac{4}{3}\frac{E\sqrt{R}}{1-\nu^2}(d-d_x)^{1.5} \quad (2)$$

The fitted fast-rate curves were then shifted by $d_x - d_0$, in order to achieve the alignment of the second-step part of the indentation curves, Fig. 4b. In principle, any other model or function that accurately describes the force-indentation development (e.g. JKR [38], DMT [39]) could be used for fitting and subsequent alignment of the curves [35]. Moreover, the method can also be applied to thin layers on hard substrates (e.g. polymer brushes). In this case, if indented to the hard substrate, the second step would show a singularity that could also be used for the alignment purposes.

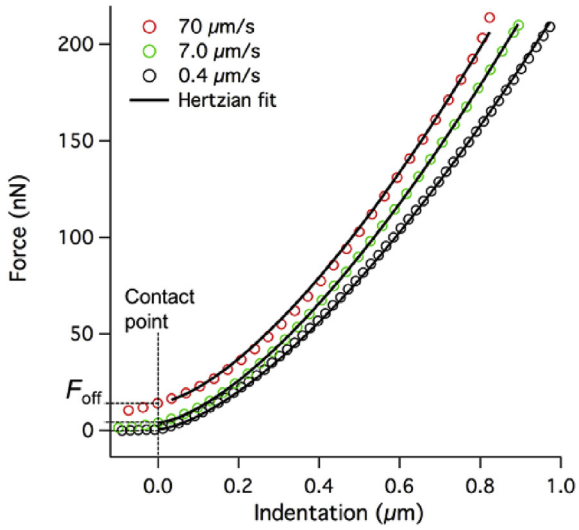

Fig. 6. First-step part of the representative force-indentation curves fitted using the Hertzian model. For clarity, only every 10th and every 100th point is shown for the curves obtained at the nominal rates of 7.0 and 0.4 μm/s, respectively.

After alignment, one might notice that the force measured at zero indentation, i.e. at the contact point, for all fast-rate indentations is larger than zero, Figs. 5b and 6. Specifically, this force offset increases with increasing indentation rate due to forces originating from the liquid drainage from the space between the probe and the sample surface. It is this exact drainage force that obscures the point of contact in conventional single-step indentation experiments, Fig. 3. Prediction of the drainage forces is theoretically possible using Reynolds equation, which was employed in the models of Vinogradova [25], for example. However, several phenomena such as surface roughness, surface slip and permeation have a great effect on the drainage forces and therefore make their prediction tedious and unreliable. A discussion and analysis of the drainage forces is included in the Supplementary information. Using the method presented here, however, we could obviate the identification of the phenomena that affect the drainage forces. We were able to determine the point of contact at each rate of indentation and take into account the generated force offset. The results of the alignment of the force curves and the determination of the rate-dependent stiffening are presented and discussed in the following section.

3. Results and discussion

Fig. 5a presents representative force curves as a function of time, where the time axis was set for each curve such that the force set-points F_{max} (or beginnings of the dwell periods) coincide. For clarity, of all the rates used in this study only the measurements obtained at the nominal rates of 0.4, 7.0 and 70 μm/s are depicted. The same set of force curves is plotted as a function of indentation depth in Fig. 5b. One can notice the overlapping parts of the second steps, which were used for the alignment of the curves, as described earlier. Characteristic poro-viscoelastic stiffening for increasing rates of indentation applied during the first step of indentation, as well as contact-force offsets can be clearly identified.

Fig. 6 shows the indentation part of the three force curves from Fig. 4b. All measured data points are shown for the curve obtained at the highest rate of about 70 μm/s, whereas only every 10th and every 100th point is shown for the curves obtained at the nominal rates of 7.0 and 0.4 μm/s, respectively. The curves were fitted (solid black lines) using the Hertzian model from Equation (1), where the

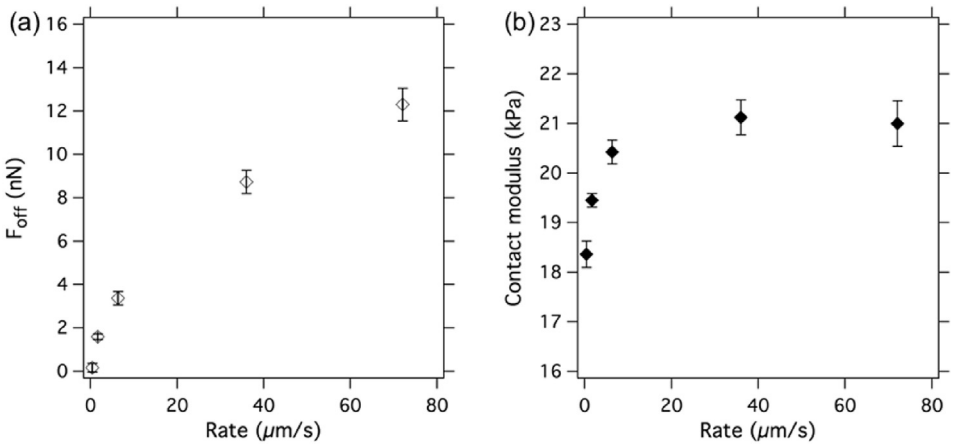

Fig. 7. (a) Measured force offset at the point of contact at different indentation rates due to the drainage of the liquid between the colloid and the hydrogel surface. (b) Effective contact moduli as a function of indentation rate, determined from Hertzian fits of the indentation curves originating at the unobscured point of contact.

contact force offset F_{off} was taken into account as:

$$F - F_{off} = \frac{4}{3}\frac{E\sqrt{R}}{1-\nu^2}(d-d_0)^{1.5}. \quad (3)$$

F_{off} was individually determined for each measured and aligned force curve by linear interpolation of the two data points closest to the contact point. The fits to the data are presented as black lines in Fig. 6. The slow-rate indentation curve (0.4 μm/s) showed good agreement with the Hertzian model, suggesting a homogeneous structure of the tested hydrogel in the first 1 μm of depth. Also the curves at fast rates showed good agreement with the model, revealing uniform stiffening throughout the entire indentation depth.

Fig. 7a and b shows average force offsets F_{off} and fitted moduli E, respectively, as functions of indentation rate. The lowest value of F_{off} corresponds to the slow-rate indentation curve and is basically the force that was used to determine the point of contact. The force offsets increased monotonically with indentation rate, reaching a value of about 12 nN at the highest rate. These are non-negligible values, considering the range of forces commonly explored during the AFM nanoindentation, indicating that strong squeeze-out phenomena are occurring at increasing rates of indentation between a probe and a sample surface. These effects might indeed be negligible for sharp AFM tips in low viscosity liquids, however, liquid squeeze-out becomes increasingly important in more viscous fluids and for larger indenter sizes since the squeeze-out forces scale linearly with viscosity and as the square of the probe radius [25].

Despite the fact that the depth of the first indentation step could be selected somewhat arbitrarily, a few limitations should nevertheless be considered. If the maximum force reached during the first indentation step is much larger than the force offset induced by the squeeze-out at the contact point ($F_{max} >> F_{off}$), the assumption of constant F_{off} throughout the indentation depth is a good approximation. However, for F_{max} that is comparable to F_{off} one should consider deriving the evolution of squeeze-out forces for an immersing (indenting) sphere. On the other hand, the maximum indentation depth is usually limited by the maximum strain, for any given model to be valid. For example, a Hertzian model could be applied for indentations up to 20% strain ($\varepsilon = \sqrt{d/R}$), meaning that the indentation depth should stay below the value of 0.04*R, where R is the probe radius. However, for materials with a Poisson's ratio around 0.4–0.5 (e.g. hydrogels), this limit could be significantly higher and up to 50% strain or 0.25*R [40]. In this work, indentation depths below 0.03*R were used, enabling the use of Hertzian contact mechanics.

The moduli shown in Fig. 7b were obtained from Hertzian fits, as shown in Fig. 6, after subtracting the rate-dependent force offsets, allowing evaluation from the unobscured point of contact. The elastic modulus of the sample hydrogel, obtained from the slow-rate curve, had a value of 18.4 kPa ± 0.3 kPa with $R^2 = 0.999$, while moduli increased up to a value of 21.1 kPa ± 0.4 kPa with $R^2 = 0.997$ at a nominal rate of 40 μm/s. No further increase was observed at a rate of 70 μm/s. Despite the modest increase of the modulus (about 12%) compared to that observed for polymer brushes or biological tissues, such as cartilage [5,8,13], the method still enables one to resolve poro-viscoelastic stiffening, even for materials showing predominantly elastic behavior. Comparable, moderate increases in storage modulus with increasing driving frequency for similar PAAm gels have also been observed by Nalam at al. [41], for both frequency-modulated (FM) nanoindentation and rheology. However, despite the remarkable matching of the data in the overlapping frequency regions between FM nanoindentation and rheology, they mention no noticeable changes in the modulus at different indentation rates for conventional nanoindentation. This could quite possibly be due to the issues in contact-point determination discussed in our work. The method presented here therefore not only enables substantial resolution in studying rate-dependent stiffening effects of soft gels, but also shows values that fall in line with other methods such rheology, for example.

4. Conclusions

We have developed a 2-step nanoindentation method to accurately align finite-rate indentation curves with respect to the contact point of quasi-static indentation of soft materials such as hydrogels in a liquid. After a finite-rate indentation and relaxation, the method uses a slow, second step of indentation for the unambiguous depth alignment of the indentation curves. This allows one to identify and take into account the force offset that appears due to the hydrodynamic drainage of the fluid confined between the probe and the sample surface.

The method was demonstrated on a PAAm hydrogel, showing that non-negligible drainage forces may appear during colloidal-probe nanoindentation. These forces should especially be taken into account in the case of viscous liquids and larger indenter sizes. Identifying squeeze-out forces in our case, allowed us to clearly resolve the rate-dependent contact moduli, despite the relatively

modest poro-viscoelastic contribution in the sample hydrogel.

Therefore, the method represents an enabling approach for the alignment of finite-rate indentation curves during indentation of soft hydrogels in liquid environments, and allows the study of material properties beyond the point of contact, such as rate- and depth-dependent stiffening effects, as well as the drainage forces ahead of contact.

Associated content

Author contributions

The manuscript was written through contributions of all authors. All authors have given approval to the final version of the manuscript. ‡These authors contributed equally.

Funding sources

This project has received funding from the European Research Council under the European Union's Horizon 2020 research and innovation programme (grant agreement No 669562). The financial support of the ETH Research Commission and the ETH Foundation are also gratefully acknowledged.

Acknowledgment

The authors wish to express their gratitude to Yvonne Gombert and Lucile Michels for the fabrication of the hydrogels.

Appendix A. Supplementary data

Supplementary data related to this article can be found at https://doi.org/10.1016/j.polymer.2018.01.017.

References

[1] A. Moore, D. Burris, Tribological rehydration of cartilage and its potential role in preserving joint health, Osteoarthritis Cartilage 25 (1) (2017) 99–107.
[2] R. Crockett, Boundary lubrication in natural articular joints, Tribol. Lett. 35 (2) (2009) 77–84.
[3] G.A. Ateshian, The role of interstitial fluid pressurization in articular cartilage lubrication, J. Biomech. 42 (9) (2009) 1163–1176.
[4] V.J. Baro, et al., Functional characterization of normal and degraded bovine meniscus: rate-dependent indentation and friction studies, Bone 51 (2) (2012) 232–240.
[5] A. Moore, D. Burris, An analytical model to predict interstitial lubrication of cartilage in migrating contact areas, J. Biomech. 47 (1) (2014) 148–153.
[6] R. Krishnan, M. Kopacz, G.A. Ateshian, Experimental verification of the role of interstitial fluid pressurization in cartilage lubrication, J. Orthop. Res. 22 (3) (2004) 565–570.
[7] F.C. Linn, Lubrication of animal joints: II the mechanism, J. Biomech. 1 (3) (1968) 193–205.
[8] E. Bonnevie, et al., Fluid load support during localized indentation of cartilage with a spherical probe, J. Biomech. 45 (6) (2012) 1036–1041.
[9] R.A. Brand, Joint contact stress: a reasonable surrogate for biological processes? Iowa Orthop. J. 25 (2005) 82.
[10] L. Han, et al., Time-dependent nanomechanics of cartilage, Biophys. J. 100 (7) (2011) 1846–1854.
[11] O. Sterner, et al., Tribological classification of contact lenses: from coefficient of friction to sliding work, Tribol. Lett. 63 (1) (2016) 1–13.
[12] M. Roba, et al., Friction measurements on contact lenses in their operating environment, Tribol. Lett. 44 (3) (2011) 387.
[13] R.M. Espinosa-Marzal, R.M. Bielecki, N.D. Spencer, Understanding the role of viscous solvent confinement in the tribological behavior of polymer brushes: a bioinspired approach, Soft Matter 9 (44) (2013) 10572–10585.
[14] R.M. Bielecki, et al., Lubrication with oil-compatible polymer brushes, Tribol. Lett. 45 (3) (2012) 477–487.
[15] R.M. Bielecki, M. Crobu, N.D. Spencer, Polymer-brush lubrication in oil: sliding beyond the stribeck curve, Tribol. Lett. 49 (1) (2013) 263–272.
[16] R.M. Bielecki, P. Doll, N.D. Spencer, Ultrathin, oil-compatible, lubricious polymer coatings: a comparison of grafting-to and grafting-from strategies, Tribol. Lett. 49 (1) (2013) 273–280.
[17] R. Heeb, et al., Room-temperature, aqueous-phase fabrication of poly (methacrylic acid) brushes by UV-LED-induced, controlled radical polymerization with high selectivity for surface-bound species, Macromolecules 42 (22) (2009) 9124–9132.
[18] S. Lee, et al., Boundary lubrication of oxide surfaces by poly (L-lysine)-g-poly (ethylene glycol)(PLL-g-PEG) in aqueous media, Tribol. Lett. 15 (3) (2003) 231–239.
[19] S.-k. Ahn, et al., Structural evolution of polylactide molecular bottlebrushes: kinetics study by size exclusion chromatography, small angle neutron scattering, and simulations, ACS Macro Lett. 3 (9) (2014) 862–866.
[20] A. Halperin, E. Zhulina, Atomic force microscopy of polymer brushes: colloidal versus sharp tips, Langmuir 26 (11) (2010) 8933–8940.
[21] H.-J. Butt, et al., Steric forces measured with the atomic force microscope at various temperatures, Langmuir 15 (7) (1999) 2559–2565.
[22] G. Scarcelli, et al., Noncontact three-dimensional mapping of intracellular hydromechanical properties by Brillouin microscopy, Nature Methods 12 (12) (2015) 1132–1134.
[23] M. Chyasnavichyus, S.L. Young, V.V. Tsukruk, Probing of polymer surfaces in the viscoelastic regime, Langmuir 30 (35) (2014) 10566–10582.
[24] S. Granick, Motions and relaxations of confined liquids, Science 253 (5026) (1991) 1374.
[25] O.I. Vinogradova, Drainage of a thin liquid film confined between hydrophobic surfaces, Langmuir 11 (6) (1995) 2213–2220.
[26] C.H. Mathis, et al., Indentation of Solvated Polymer Brushes: Identifying the Point of Contact, 2017. Submitted for publication.
[27] E. Charrault, et al., Boundary flow on end-grafted PEG brushes, Soft Matter 12 (6) (2016) 1906–1914.
[28] H.-J. Butt, M. Jaschke, Calculation of thermal noise in atomic force microscopy, Nanotechnology 6 (1) (1995) 1.
[29] R.J. Cannara, M. Eglin, R.W. Carpick, Lateral force calibration in atomic force microscopy: a new lateral force calibration method and general guidelines for optimization, Rev. Sci. Instrum. 77 (5) (2006), 053701.
[30] O.I. Vinogradova, G.E. Yakubov, Surface roughness and hydrodynamic boundary conditions, Phys. Rev. 73 (4) (2006), 045302.
[31] A. Sommerfeld, Ein beitrag zur hydrodynamischen erklaerung der turbulenten fluessigkeitsbewegungen, Atti del 4 (1908) 116–124.
[32] G.K. Batchelor, An Introduction to Fluid Dynamics, Cambridge university press, 2000.
[33] O.I. Vinogradova, et al., Dynamic effects on force measurements. I. Viscous drag on the atomic force microscope cantilever, Rev. Sci. Instrum. 72 (5) (2001) 2330–2339.
[34] O.I. Vinogradova, G.E. Yakubov, Dynamic effects on force measurements. 2. Lubrication and the atomic force microscope, Langmuir 19 (4) (2003) 1227–1234.
[35] D.C. Lin, F. Horkay, Nanomechanics of polymer gels and biological tissues: a critical review of analytical approaches in the Hertzian regime and beyond, Soft Matter 4 (4) (2008) 669–682.
[36] P. Attard, Measurement and interpretation of elastic and viscoelastic properties with the atomic force microscope, J. Phys. Condens. Matter 19 (47) (2007) 473201.
[37] H.R. Hertz, Über die Berührung fester elastischer Körper und über die Härte, 2006.
[38] K. Johnson, K. Kendall, A. Roberts, Surface energy and the contact of elastic solids, in: Proceedings of the Royal Society of London a: Mathematical, Physical and Engineering Sciences, 1971.
[39] B.V. Derjaguin, V.M. Muller, Y.P. Toporov, Effect of contact deformations on the adhesion of particles, J. Colloid Interface Sci. 53 (2) (1975) 314–326.
[40] E. Yoffe, Modified Hertz theory for spherical indentation, Phil. Mag. 50 (6) (1984) 813–828.
[41] P.C. Nalam, et al., Nano-rheology of hydrogels using direct drive force modulation atomic force microscopy, Soft Matter 11 (41) (2015) 8165–8178.